Project No: 603502

DACCIWA

"Dynamics-aerosol-chemistry-cloud interactions in West Africa"

Deliverable

D7.3 Forecast Evaluation

Due date of deliverable:	30/04/2017
Completion date of deliverable:	30/05/2017
Start date of DACCIWA project:	1st December 2013 **Project duration:** 60 months
Version:	[V1.0]
File name:	[D7.3_Forecast_Evaluation_DACCIWA_v1.0.pdf]
Work Package Number:	**7**
Task Number:	**3**
Responsible partner for deliverable:	**MO**
Contributing partners:	**KIT, ECMWF, ETHZ**
Project coordinator name:	Prof. Dr. Peter Knippertz
Project coordinator organisation name:	Karlsruher Institut für Technologie

The DACCIWA Project is funded by the European Union's Seventh Framework Programme for research, technological development and demonstration under grant agreement no 603502.

Dissemination level		
PU	Public	**x**
PP	Restricted to other programme participants (including the Commission Services)	
RE	Restricted to a group specified by the consortium (including the Commission Services)	
CO	Confidential, only for members of the consortium (including the Commission Services)	

Nature of Deliverable		
R	Report	**x**
P	Prototype	
D	Demonstrator	
O	Other	

DOCUMENT INFO

Authors

Author	Beneficiary Short Name	E-Mail
Angela Benedetti	ECMWF	Angela.Benedetti@ecmwf.int
Anke Kniffka	KIT	anke.kniffka@kit.edu
Peter Knippertz	KIT	P.Knippertz@leeds.ac.uk
Marlon Maranan	KIT	marlon.maranan@kit.edu
Konrad Deetz	KIT	konrad.deetz@kit.edu
Malcolm Brooks	UK MO	malcolm.e.brooks@metoffice.gov.uk
Peter Hill	Uni Reading	p.g.hill@reading.ac.uk

Changes with respect to the DoW

Issue	Comments
Delay of one month	This Deliverable required a large amount of model and observational data to be processed. While doing this we encountered a number of software and incompatibility problems that have slowed down progress more than we expected. The delay was approved by the PO on 06.04.2017

Dissemination and uptake

Target group addressed	Project internal / external
Public scientific community	Internal and external

Document Control

Document version #	Date	Changes Made/Comments
0.1	20.03.2017	Template
0.2	12.05.2017	Draft
0.3	16.05.2017	Version for approval by the general assembly
0.4	29.05.2017	Final editions
1.0	30.05.2017	Final version approved by the general assembly

Table of Contents

1 Introduction

In Deliverable D7.2 forecast activities for the main DACCIWA field campaign in June-July 2016 were described. The purpose of the present Deliverable D7.3 is to document the evaluation of these forecasts using available data from standard networks and satellites as well as data from the field campaign where already available (particularly radiosondes). Digitisation efforts for meteorological stations run by West African weather services for 2016 are still ongoing and thus are not used in this document but will be in future scientific investigations of the campaign period. The evaluation covers a range of meteorological variables using a variety of graphical displays and scores also used in operational services. To the best of our knowledge, this is the first attempt ever to systematically evaluate a range of operational and research models (including some with convection-permitting resolution) run in weather forecast mode over the southern West African region. The document is structured as follows: Section 2 provides a summary description of all the modelling systems participating in this exercise, while section 3 gives information on the observational datasets used for evaluation (mostly stations, radiosondes and satellites). Some selected graphical and statistical results are shown in Section 4 to illustrate the range of evaluation products produced and analysed. Finally, a short summary, conclusions and an outlook is given in section 5.

2 Evaluation strategy

2.1 Choice of models and data sources

In a first step, we examined all models that qualify to be part of the evaluation procedure. We selected models that are either operational (such as the European Centre for Medium-Range Weather Forecasts (ECMWF)'s Integrated Forecast System) or that are used for research within the DACCIWA project. Figure 1 gives a list of all models considered at the planning stage. Of specific interest are models that exist in those two versions, e.g. ICON operational from the German Weather Service (DWD) or as research version at KIT. The grid spacing of the selected models (delta x in Figure 1) ranges from 3 to 75 km, implying that some allow for explicit moist convection and other employ parameterisations.

	A	B	C	D	E	F	G	H	I	J	K
1	**Forecast evaluation D7.3 (June & July 2016 only, forecast day +1 and +2)**										
2											
3	**type**	**model**	**delta x**	**delta t output**	**Time span**	**Tendencies**	**Integration**	**convective**	**2-way coupling**	**status**	**Contact**
4	research	**WRF (version 3.3.1)**	3 km	1 h	A,M,J,J,A,S,O	T,q,u,v	12 UTC + 54 h	X	O in nest	planned	M. Maranan
5	research	**COSMO (version 5.1)**	25 km	3 h	J,J	X	12 UTC + 57 h	O	X	done	K. Deetz
6	operational	**ICON (version 2.0.15)**	13 km	3 h	J,J	X	12 UTC + 57 h	O	global	done	A. Kniffka / K. Deetz
7	research	**ICON (version 2.0.12)**	6.5 km	1 h	J,J (+A,S)	T,q,(u,v)	00 & 12 UTC +≥120h	X	O in nest	planned	A. Kniffka
8	operational	**ECMWF IFS (CY41R2)**	9 km	1 h first 90 h, 3 h after that	J,J (+more)	X	00 & 12 UTC +≥120h	O	global	available	A. Benedetti
9	research	**ECMWF IFS (CY43R1)**	16 km	3 h	J, J	T,q,u,v	00 UTC + 36h	O	global	done	A. Benedetti
10	re-analysis	**ERA-Interim (CY31R2)**	75km	3h	J, J (+more)	X	00 & 12 UTC +≥120h	O	global	available	A. Benedetti
11	research	**UM (version 8.3)**	4 km	1 h	J, J	T,q	12 UTC +72h	X	X	done	P. Rosenberg
12	operational	**UM (OS37)**	17 km	Varies by field, typically 1h first 48 hours, 3 h after that	J, J (+AMS)	Checking status	00, 12Z +144h, 06, 18Z +72h	O	global	available	M. Brooks
13											

Figure 1: List of models to be compared in the evaluation exercise.

Together with researchers from WP5 (Radiative Processes) we discussed the advantages and disadvantages of possible comparison data sources such as radiosondes or satellite sensors in the context of suitability for southern West Africa. Figure 2 provides a list of different data sources considered (first column) and the meteorological variables they could provide (following columns). After some testing, not all considered products were used in the end. A drawback for many satellite sensors for example is the persisting and thick high cloud cover that obscure clouds close to the surface and handicap the derivation of solar surface radiation. This has to be taken into account for the discussion. We chose data sources that

were a) particularly suitable for the evaluation and b) available during the time of the campaign in high temporal resolution and sufficient quality.

	precip	cloud fraction	LWP/IWP	CTT	TPW	surface sol. rad	TOA rad	T2m/Td2m	v10m	p	q
TRMM 3B42	(1,3)(F,G,H,I)	x	x	x	x	x	x	x	x	x	x
GPM	(1,3)(F,G,H,I)	x	(1,3)(F,G,H,I)	x	x	x	x	x	x	x	x
GPM constellation	?	x	?	x	?	x	x	x	x	x	x
GPM_3GPROFMT1S	?	x	?	x	?	x	x	x	x	x	x
GPCC/P	(F,H)	x	x	x	x	x	x	x	x	x	x
CLAAS	x	(1,3)(F,G,H,I)	(1,3)(F,G,H,I)	(1,3)(F,G,H,I)	x	x	x	x	x	x	x
NASA-Langley-Geo		?	?	?	x	?	x	x	x	x	x
GERB	x	x	x	x	x	x	(1,3)(F,G,H,I)	x	x	x	x
MODIS (Terra/Aqua)		(1,3)(G/I)	(1,3)(G/I)		(1,3)(G/I)	x	x	x	x	x	x
GEOPROF	x	3(G,H,I)	3(G,H,I)	3(G,H,I)	x	x	x	x	x	x	x
SSMI, AVHRR, MHS	x	x	x	x	(1,3)(A/B,C/D)	x	x	x	x	x	x
SYNOP/METAR	(1,3)(F,G,H,I)	(1,3)(F,G,H,I)	x	x	x	x	x	(1,3)(F,G,H,I)	(1,3)(F,G,H,I)	(1,3)(F,G,H,I)	x
Rad. Stations	x	x	x	x	x	(1,3)(F,G,I)	x	x	x	x	x
Upper–air	x	x	x	x	x	x	x		x	(2,5)(F,G,H,I)	(2,5)(F,G,H
Field sites	(1,3)(F,G,H,I)	(1,3)(F,G,H,I)	(1,3)(F,G,H,I)	x	x	(1,3)(F,G,H,I)	x	(1,3)(F,G,H,I)	(1,3)(F,G,H,I)	(1,3)(F,G,H,I)	(1,3)(F,G,H
AMMA catch	x	x	x	x	x		x		?		x
large aircraft	x	(1,2)l	(1,2)l	x	x	x	x	x	x	(1,2)l	(1,2)l

x= not suitable | are daylight averages

Figure 2: Sources of possible evaluation data during the discussion (first column) and parameters of interest (following columns). The numbers and letters in the individual cells stand for temporal and spatial averages as detailed in the Appendix. Not all data listed here were used in the end, sources marked with a "?" were excluded since they turned out not to be suitable for the evaluation.

2.2 Planning of the evaluation procedure

Due to the large number of models and comparison data we developed a strategy to fulfil the evaluation tasks in due time.

In order to reach the maximum amount of comparable models and parameters we distributed the workload amongst all project partners. In general, one person was responsible for all parameters from one model and/or one observational source. This also depended on the already existing archived model or satellite data. We developed a processing guideline, which all partners used (see Appendix). In this guideline, common metrics, horizontal grid resolution, vertical levels, hours of forecast and other parameters were prescribed as well as a naming convention. Together with the guideline, an evaluation software package was developed to ensure easy comparability.

The partners applied the software to reformat the data sets so that they all have the same structure and follow a specific naming convention, which makes automatic comparison possible. All the data sets that were prepared in this manner were then delivered to ECMWF for the actual evaluation. This is a novel approach to compare multi-scale models over a common region.

2.3 Data processing script

As mentioned in section 2.2., to process data from the different sources in a efficient and consistent way, a script was developed and shared between the involved partners. This shell script uses the Climate Data Operators that can process all kinds of model data given in netcdf format. The script performs all necessary preparatory tasks such as re-gridding, geographical truncation, averaging in time and space etc. The processed datasets possess the properties listed below:

Area: 8°W–8°E, 5–10°N

Grid: 0.2° x 0.2°

Pressure levels: 100, 150, 200, 250, 300, 350, 400, 450, 500, 550, 600, 650, 700, 750, 800, 850, 900, 925, 950, 975, 1000

Runs: 54 h runs were conducted, with 6h of spin-up, simulations were started at 12 UTC, 3 hourly output

Temporal averages: pre- and post-monsoon onset (following the definition introduced in Knippertz et al. 2017) period averages, daily averages, average diurnal cycles, 3 hourly data

Spatial averages: DACCIWA region as box average (purple box in Figure 3) and individual stations (Figure 3)

Naming convention: Detailed information on the automatic filename assignment can be found in the Appendix.

Figure 3: Geographical overview of DACCIWA focus region (taken from recently submitted overview paper of Flamant et al., BAMS). The purple box shows the area used for spatial averaging (8°E–8°W, 5–10°N). Ground-sites, aircraft base, radiosonde stations and other geographical features of interest are marked.

2.4 Plotting and verification metrics

After the pre-processing described in section 2.3 all data were delivered to ECMWF, where they were further processed using python scripts. Despite the fact that all data had the same format (netcdf) and the same variables, there were still residual difference in the names of the variables and units, which made the post-processing more challenging than anticipated.

A key tool for the actual verification was the software “verif” available at https://github.com/WFRT/verif (courtesy of Thomas Nipen and collaborators, MetNo) and used operationally at ECMWF. The standard configuration for this tool is to process ECMWF output alone and thus an adaptation to several different models became necessary. The SYNOP data used in the station verification were extracted from the ECMWF Meteorological Archival and Retrieval System (MARS) archive and also processed with the same python scripts. Files with the multi-model fields and the observations were created and input to the “verif” software. All 2D variable statistics and plots were produced using this tool.

3 Description of participating models

3.1 COSMO-ART (KIT)

3.1.1 Model description

COSMO-ART (Consortium for Small-scale Modeling – Aerosols and Reactive Trace gases) is a comprehensive online-coupled model system (Vogel et al., 2009) based on the operational weather forecast model COSMO (Baldauf et al., 2011). COSMO-ART includes a comprehensive chemistry module to describe the gaseous composition of the atmosphere and secondary aerosol formation. It allows for feedback of the simulated aerosol particles with radiation, cloud formation and precipitation (e.g. Stanelle et al., 2010, Athanasopoulou et al., 2014; Rieger et al., 2014; Walter et al., 2016). The size distribution of aerosol within COSMO-ART is approximated by log-normal distributions. The standard deviation is kept constant while the median diameter of the aerosol changes during transport. Chemical reactions are calculated with RADMKA (Regional Acid Deposition Model Version Karlsruhe; Vogel et al., 2009), which is based on RADM2 (Regional Acid Deposition Model, Stockwell et al., 1990). The formation of secondary organic aerosol is calculated by a VBS approach (volatility basis set; Athanasopoulou et al., 2013). COSMO-ART explicitly treats the aging of soot particles transferring them from external to internal mixtures as described in Riemer et al. (2004).

Radiative fluxes are calculated with the GRAALS radiation scheme (Ritter and Geleyn, 1992). A priori Mie calculations have been performed for the initial aerosol particle size distributions and their chemical composition to obtain mass-specific values for the extinction coefficient, single scattering albedo, and asymmetry parameter. These coefficients also depend on wavelength. To consider the optical properties of the current aerosol distribution the mass-specific parameters obtained by the Mie calculation are weighted with the mass fraction of the chemical components. A full two-moment cloud microphysics scheme (Seifert and Beheng, 2006) is used. Aerosol activation is considered according to Fountoukis and Nenes (2005). Ice nucleation is based on the parametrization by Phillips et al. (2008). Cirrus formation and the competition between homogeneous and heterogeneous freezing is specified according to Barahona and Nenes (2009a, b).

COSMO-ART is able to describe the emission and atmospheric dispersion of natural (mineral dust, sea salt, volcanic ash, biogenic volatile organic compounds and pollen) and anthropogenic pollutants (anthropogenic emissions e.g. from traffic or industry, biomass burning emissions including a plume rise model (Walter et al., 2016) and flaring emissions).

3.1.2 Adaptations for DACCIWA

To apply COSMO-ART to the conditions of SWA, several adaptations have been realized. The global EDGAR emission database was preprocessed for COSMO-ART and the biogenic emission routine MEGAN2.1 of Guenther et al. (2012) was implemented into COSMO-ART, allowing state-of-the-art calculation of biogenic emissions of isoprene, limonene and alpha-pinene depending on current meteorological (radiation and temperature) and land surface (leaf area and plant functional types) conditions. Additionally we have further developed our mineral dust emission routine. By combining the parameterization of Vogel et al. (2009) and Shao et al. (2010) the emission routine can now be flexible applied globally compared to the previous scheme in COSMO-ART. The external emission dataset for oceanic dimethyl sulfide (DMS) was updated using Lana et al. (2011). In COSMO-ART the DMS emission depends on wind speed. Not considered are NO_x emissions from lightning and soil. For anthropogenic emissions we use EDGAR HTAP V2 (EDGAR, 2010) and for the biomass burning emissions the CAMS

Global Fire Assimilation System (GFAS, 2016), which is available in near real-time. We use the tropical setup with includes among others an increased number of vertical levels up to 30km.

3.1.3 COSMO-ART forecasts

As a part of the DACCIWA measurement campaign (June-July 2016) and especially the aircraft campaign (27 June to 17 July 2016) COSMO-ART operational aerosol/chemistry forecasts were realized from 8 May to 31 July 2016. With that we supported the decision-making of the flight planning during the campaign. The forecast visualization was regularly uploaded to the campaign server (http://dacciwa.sedoo.fr/source/indexItem.php?current=20161109&nav=COSMO-ART), which can also be used for post-campaign decisions about case studies. As meteorological driver, ICON forecasts were provided by the German Weather Service. The model forecast setup is summarized in Table 1.

Table 1: Characteristics of the COSMO-ART forecast model setup

Characteristics	**Dataset**
Time period	01.06.-31.07.2016
Simulation domain	25°W – 40°E, 20°S – 35°N
Grid mesh size (km)	28
Number of vertical levels	50
Meteorological boundary conditions	ICON
Convection parameterization	yes
Cloud microphysics	one-moment bulk
Aerosol type (online/prescribed)	mineral dust (online), sea salt (online), anthropogenic (prescribed)
Aerosol treatment (bulk/modal/sectional)	modal
Direct aerosol effect	climatology
Indirect aerosol effect	prescribed CCN
Chemical boundary conditions	MOZART
Chemistry (online/prescribed, full chemistry)	online, full chemistry

3.2 ICON (DWD + research version at KIT)

3.2.1 Operational version at DWD

ICON (Icosahedral Nonhydrostatic, Zängl et al., 2014) is a global numerical weather prediction model recently developed by the Max Planck Institute for Meteorology (MPI-M) and the German Weather Service (DWD). Since January 2015, it is operationally used at the DWD for global predictions. ICON's horizontal grid is based on triangles that cover the globe so that the area of the triangles remains approximately equal everywhere. It is an Arakawa C type grid, which has the distinction of high scalability and easily possible nesting.

Currently, ICON is operated with a global horizontal mesh size of 13 km and 90 vertical levels, with 11 levels up to the first 1000 m (zero topography height). The vertical coordinate is height-based and terrain following in the lower levels but is smoothed in the upper troposphere via the application of a SLEVE coordinate (Leuenberger et al., 2010).

For the dynamical core the continuity equation is formulated in the flux form with density as the prognostic variable in order to achieve mass conservation as close as possible. This enables exact local mass conservation and mass-consistent tracer transport. The equations are solved non-hydrostatically on the global domain. The time integration is performed with a two-time-level predictor–corrector scheme. Apart from the sound wave propagation, this scheme is fully explicit.

ICON has several physical packages that can be chosen. The physics packages that are currently used at DWD are shortly summarized: the fast physics package are inherited from the COSMO model (Doms and Schättler, 2004) but partly reformulated for ICON. The cloud microphysics scheme is the COSMO-EU five-category prognostic scheme (Doms and Schättler, 2004; Seifert, 2008) adapted for ICON with the extension of ice sedimentation. The turbulence scheme by Raschendorfer (2001) solves the prognostic equation for turbulent kinetic energy and for the land-surface interaction TERRA is used in an updated version (Heise, 2006). For the slow developing physics, the Bechtold et al. (2008) convection scheme, the Lott and Miller (1997) subgrid-scale orography scheme and the Orr et al. (2010) non-orographic gravity-wave drag scheme are applied. Radiative transfer is solved with the Rapid Radiation Transfer Model (RRTM) radiation scheme (Mlawer et al., 1997) where a greens function approach is applied for solar bands with approximated diffuse radiation (Barker et al., 2002). The slow-physics parametrizations correspond to the ones from the Integrated Forecasting System (IFS) of the ECMWF.

The results presented in this report were all created from non-ensemble runs. The DWD has ensemble runs for the highly resolved COSMO model in the Germany domain, but global ensemble sets are still under construction. Data assimilation, however, is realized as an ensemble assimilation system for the global runs since January 2016. This is a hybrid combination of an ensemble Kalman filter together with a variation procedure.

3.2.2 Research version from KIT

The research version of KIT corresponds to the ICON operational version but it does not have the data assimilation from DWD. In contrast, it is initialized with analysis fields from ECMWF IFS for each start of a 54 h run. The model was started with a set-up similar to the operational version with the exception of some flags that are specifically useful for tropical environments (e.g. reduction of the moist bias in the lower tropical atmosphere).

3.3 IFS (ECMWF)

3.3.1 Recent updates to ECMWF operational system

On 8 March 2016, ECMWF upgraded the horizontal resolution of its integrated forecasting system (IFS) including its high-resolution (HRES) and ensemble (ENS) forecasts. The upgraded horizontal resolution is about 9 km for the HRES and the data assimilation (the outer loop of the 4D-Var) and about 18 km for the ENS up to day 15 and about 36 km for the extended range (monthly). The resolution of the ensemble of data assimilations (EDA) is increased to 18 km.

A new cycle of the IFS has been introduced to implement the horizontal resolution upgrade. This includes a number of enhancements to the model and data assimilation. The main contents are:

1. Increased horizontal resolution: this was achieved by using a cubic reduced Gaussian grid (with spectral truncation denoted by TC) instead of the former linear reduced Gaussian grid (denoted by TL). With the cubic reduced Gaussian grid the shortest resolved wave is represented by four rather than two grid points. In addition, a new form of the reduced Gaussian grid, the octahedral grid, is used. The octahedral grid is globally more uniform than the previously used reduced Gaussian grid.
2. Higher realism of the kinetic energy spectrum: this was significantly improved with more energy in the smaller scales due to a reduction of the diffusion and removal of the de-aliasing filter, enabled by the change to using a cubic truncation for the spectral dynamics.
3. Significant revision to the specification of background error covariances (B) used in the HRES data assimilation: this is due to the increased resolution of the Ensemble Data Assimilation (EDA) and the introduction of scale-dependence of the hybrid B matrix (climatological and EDA), thereby relying more on the EDA "errors of the day" for the smaller scales.
4. Improvements in the use and coverage of assimilated satellite data: these were due to changes in observation selection and error representation (for GPS radio occultation data, all-sky microwave, AMSU-A, IASI and AMVs) and improved observation operators for radiance data from microwave sounders.
5. Improved stability of the semi-Lagrangian scheme near strong wind gradients: this reduces noise downstream of significant orography and in tropical cyclones.
6. Improved radiative heating/cooling at the surface: this was achieved by introducing approximate updates on the full resolution grid at every timestep. This leads to a reduction in 2-metre temperature errors, particularly near coastlines (relevant for DACCIWA).

Additionally there are changes to the triggering of deep convection, non-orographic wave drag and improvements to the linear physics in the data assimilation (for gravity wave drag, vertical diffusion and the surface exchange).

The documentation for the ECMWF's Integrated Forecast System (latest release) is available online at
http://www.ecmwf.int/search/elibrary/part?solrsort=sort_label%20asc&title=part&secondary_title=41r1&f[0]=ts_biblio_year%3A2016

3.3.2 ECMWF's forecasts for DACCIWA

During the 2016 flight campaign, ECMWF sent operational forecasts to the DACCIWA team via the SEDOO webpage (dacciwa.sedoo.fr) and ftp. Tailored plots of meteorological variables were produced. This is summarized in report D7.2. In parallel to the meteorological fields, aerosol and chemical variables from the Copernicus Atmosphere Monitoring Service (CAMS) operational run were also provided. CAMS is a Copernicus Service run at ECMWF. CAMS runs IFS at a lower resolution due to computational constraints. The resolution of the aerosol and chemistry fields during the DACCIWA campaign was ~80km, while the resolution of the meteorological fields was 9km. In this report only the meteorological variables are included. The validation of the aerosol and chemical variables is performed under Task 3.2. It

is worth noting that aerosols are not prognostic variables in the operational meteorological run of the ECMWF's IFS. No specific modifications were applied to IFS for the DACCIWA campaign.

3.3.3 Routine verification of the West African Monsoon at ECMWF

ECMWF routinely verifies parameters related to the West African Monsoon. This activity is not part of DACCIWA *per se* but it is relevant for the project, as it looks at the area of interest. Figure 4 shows the precipitation maps for 10 June 2016 (pre-onset) and 10 July 2016 (post-onset). Two forecast ranges are shown, 30h and 102h. Comparisons with FEWS-NOAA data available from http://www.cpc.ncep.noaa.gov. (Novella and Thiaw 2013) show that the HRES ECMWF model has a tendency to underestimate heavy precipitation and to overestimate light precipitation both before and after the onset of the West African Monsoon.

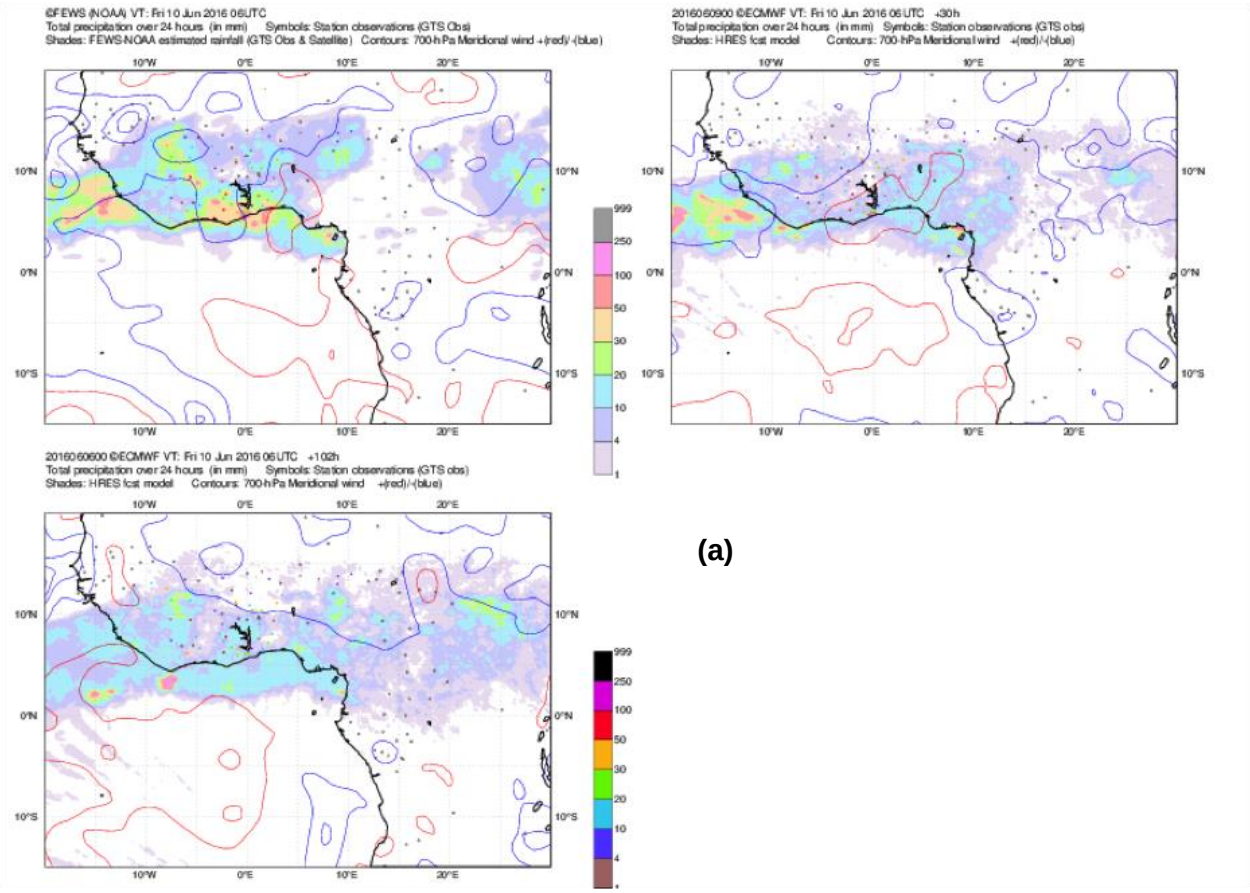

(a)

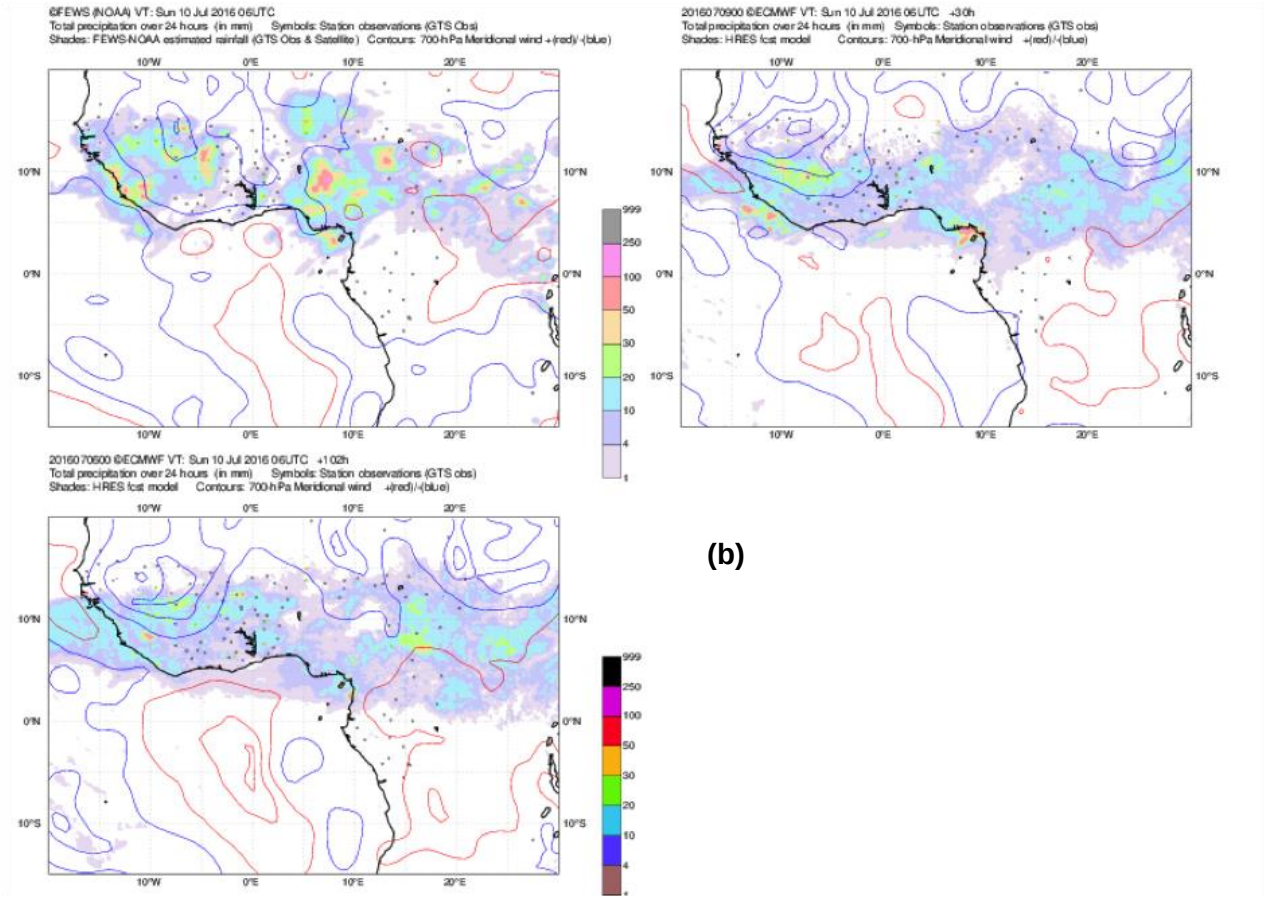

Figure 4: Exemplary precipitation maps for 10 June 2016 (a) and 10 July 2016 (b). Top left panel shows the observations, whereas the right top and the left bottom panels show the HRES ECMWF 24 accumulated precipitation for forecast ranges 30h and 102h, respectively. Plots courtesy of Fernando Prates (ECMWF).

3.4 UNIFIED MODEL (MET OFFICE)

The Met Office forecasts were provided in near real time from the operational global Numerical Weather Prediction (NWP) model running the Met Office Unified Model (MetUM) (Cullen and Davies, 1991). The MetUM has a non-hydrostatic, fully compressible, deep-atmosphere dynamical core, solved with a semi-implicit semi-Lagrangian time step on a regular latitude-longitude grid (Wood et al., 2014). The MetUM is suitable for atmospheric prediction on a wide range of temporal and spatial scales (Brown et al., 2012), from high resolution convection resolving local area models, for short range NWP, to climate change simulations running on centennial time scales. At longer timescales the model is often coupled to other models of the ocean, cryosphere, biosphere and atmospheric composition.

The scientific aspects of the global model configuration, as opposed to purely technical, are developed and documented in conjunction with that of the Met Office climate and seasonal modelling systems as a single Global Atmosphere model (GA). The same applies for the land surface component running the Joint United-Kingdom Land Environment Simulator (JULES, Best et al. (2011)) which is developed as the Global Land (GL) model. The current operational configuration is GA6.1 which is described in detail in Walter et al. (2016).

Of particular relevance to the DACCIWA region

- Sub-grid scale cumulus convection is represented with a mass-flux scheme based on Gregory and Rowntree (1990), with various extensions described in Walter et al. (2016).
- Aerosols:
    - Mineral dust is represented in the operational global NWP using a 2-bin version of Woodward (2001) with a prescribed emission size distribution. The direct effect of dust on the incoming solar and outgoing thermal radiation is included.
    - Both the direct and indirect effects, through clouds and precipitation growth, are included from climatologies generated from long-running present day climate model simulations using a full aerosol scheme (CLASSIC) described in Bellouin et al. (2011). The climatological aerosol species are: biogenic aerosols, sulphate, biomass-burning, black carbon from both biofuels and fossil fuel combustion, and sea-salt.

The current global NWP model has a resolution of 0.23º longitude by 0.16º latitude which corresponds to approximately 17 km in mid-latitudes and 26 km at the equator. The global model reaches 85km and has 70 levels.

In the global model, the standard meteorological fields initialised using a Hybrid Ensemble 4D-Var data assimilation (DA) system described in Clayton et al. (2012); Rawlins et al. (2007). The global model DA cycle is 6 hourly, with 2 main run forecasts per day, at 00Z and 12Z. Due to its computational expense the DA process is run at a lower resolution of 0.5625º by 0.375º, corresponding to approximately 40km in mid-latitudes. The model soil moisture is initialised by assimilating soil wetness observations from ASCAT on the forecast model grid (Dharssi et al., 2011). The mineral dust forecasts are updated by assimilating Aerosol Optical Depth (AOD) observations from MODIS.

3.4.1 Additional aerosol forecasts for DACCIWA

In addition to the operational NWP forecast data, an additional set of experimental forecasts were provided to DACCIWA which included additional aerosol species for flight planning purposes:

- The biomass burning aerosol scheme was enabled, but it's emissions were modified to include all primary emissions of carbonaceous aerosol (fossil-fuel, bio-fuel, biomass burning), lumped into one carbonaceous aerosol species.
- The full sulphur cycle and sulphate aerosol representation from CLASSIC was included.

Aerosol emissions were mostly derived from the MACC/CityZEN (via ECCAD-Ether at http://eccad.sedoo.fr), based on an interpolation from the historical emissions. Biomass burning aerosol emissions were taken from the Global Fire Assimilation System (GFAS) which was available in near-real time with a 1 day lag.

As an experimental forecast used to assist near-real time flight planning, the additional aerosol species were not allowed to interact with the evolution of the model; the aerosol climatologies were kept in place. For this reason the forecasts are identical between the aerosol and operational forecasts in all of the evaluated observations in this document.

3.5 WRF (KIT)

The Weather Research and Forecasting Model (WRF), version 3.3.1, together with Version 3 of the Advanced Research WRF (ARW) dynamics solver, is a fully compressible, non-hydrostatic model that is widely used in both research and numerical weather prediction (NWP) (Skamarock et al. 2008). Simulations with WRF is part of DACCIWA WP6, Task 6.2, in which the analysis of the (thermo-)dynamical causes of rainfall in the DACCIWA domain and the subsequent comparison with observation data are one of the main objectives.

3.5.1 Basic model configuration

The configuration of Schuster et al. (2013) is used where WRF was tuned towards a best possible representation of the diurnal cycle of low-level stratus in southern West Africa. Following a series of sensitivity tests of physical schemes and parameters conducted by the author, WRF runs with the following settings:

- Planetary boundary layer scheme: Mellor-Yamada-Nakanishi-Niino level 2.5 (Nakanishi & Nino, 2009)
- Number of vertical levels: 70
- Land-Surface Model: Noah LSM (Chen & Dudhia, 2001)
- Microphysics Scheme: Morrison 2-moment scheme (Morrison & Gettelman, 2008)
- Radiation scheme: Rapid Radiative Transfer Model for GCMs (Mlawer et al., 1997)

3.5.2 Settings for DACCIWA

WRF is operated with two nested domains where the two-way nested innermost domain encompasses a box ranging from 4°N to 12°N and from 10°W to 15°E with a grid spacing of 3 km. Compared to the original settings in Schuster et al. (2013) the domain was extended towards the north and east to include the Adamawa Mountains at the Nigerian-Cameroonian border and the Jos Plateau in Northern Nigeria. Recent studies (e.g. Schröder et al., 2009) have shown that both mountain ranges exhibit high convective activity that may contribute to a substantial fraction of rainfall in the DACCIWA region. The parent domain ranges from 0° to 15°N and 15°W to 20°E with a grid spacing of 9 km. For this domain, the Grell-3D parameterization for convection is applied.

3.5.3 WRF simulation series and initial/boundary conditions

Daily 54-hour integrations initialized at 12 UTC are performed over the rainy season 2016 (April–October). Operational model analysis from the ECMWF is used as initial and boundary conditions for the simulation series. For the period of the DACCIWA field campaign in June and July 2016, the analysis includes, amongst others, around 772 assimilated radiosonde profiles. During the first 6 hours of each run, the model is nudged towards the analysis in order to provide the best possible conditions for the formation of nocturnal low-level clouds in the domain.

4 Results

In this section, an illustration of the graphical evaluation products generated is given. First of all, station-wise comparisons are shown that use SYNOP measurements. Secondly, the models are evaluated against radiosonde measurements taken as part of the DACCIWA field campaign. As a last point the overall agreement for the full DACIWA box (8°E–8°W, 5–10°N) is presented based on satellite and surface data.

4.1.1 Surface Stations

Within the DACCIWA region, initial evaluation activities are focused on six stations that provided synoptic measurements during the time of the campaign: Abidjan, Accra, Kumasi, Cotonou, Parakou and Savè (see map with the location of the stations in Figure 3). Three of the stations are situated at or very close to the coast, while the others are farther inland. All stations provided regular 3-hourly measurements but some small gaps exist. In the analysis, we distinguished between the periods before the monsoon onset (01–21 June 2016) and after (22 June – 31 July 2016) (as in the recently submitted overview paper by Knippertz et al. 2017) and separated the model data into forecast Days 1 and 2, since we had 48 hours of valid simulations (+ a six hour spin-up time, see section 2).

As a first example, the temperature at the inland station Parakou is shown in Figure 5. In the upper left panel the original time-series of the six models and the observations during the pre-monsoon period are displayed for 2-m temperature on forecast Day 1. Only times when observational data were available are shown. The nomenclature for the models of this and the following legends is listed in Table 2: Colour code and names of the models and observations in the following figures. More information on models is given in Figure 1 and section 3..

Table 2: Colour code and names of the models and observations in the following figures. More information on models is given in Figure 1 and section 3.

code	**obs**	**eco**	**iop**	**irs**	**cos**	**wrf**	**ukmo**
Full name	Synop obser-vations	ECMWF IFS operatio-nal	ICON opera-tional	ICON research version	COSMO research version	WRF research version	UK met office UM operatio-nal

Since Parakou is an inland station, a comparatively strong diurnal fluctuation of about 10 K can be seen, which is reproduced in general by all models. The average diurnal cycle for this period in the upper right panel shows that most models have the lowest bias at 6 UTC. The spread (and thus also the bias for most models) is largest around noon and in the early evening, which likely mirrors to some extent the various differences in cloud production during daytime. In particular, eco and wrf are overestimating the diurnal cycle, potentially indicating too little cloud cover in the afternoon. For a more detailed analysis the Kendall correlation coefficient (bottom left in Figure 5) and the root mean square error (RMSE, bottom right) are used. The correlation gives a measure of the models' ability to reproduce day-to-day variations in temperature, while the RMSE gives the absolute deviation point-in-time-and-space-wise as a diurnal cycle.

The relatively small correlations of about 0.3 at best for all models show a general problem to reproduce the temporal evolution of temperature at Parakou, particularly at midnight and at 12 UTC. As shown by the top left panel, these day-to-day variations are relatively small and probably related to variations in cloudiness and possibly rainfall, which the models struggle to represent. In contrast to extratropical locations changes in horizontal advection, which are typically more reliable in models in general, play a less important role for this location. Together the low correlations and existing biases lead to relatively high RMSE of up to 4 K at midday (bottom right panel in Figure 5).

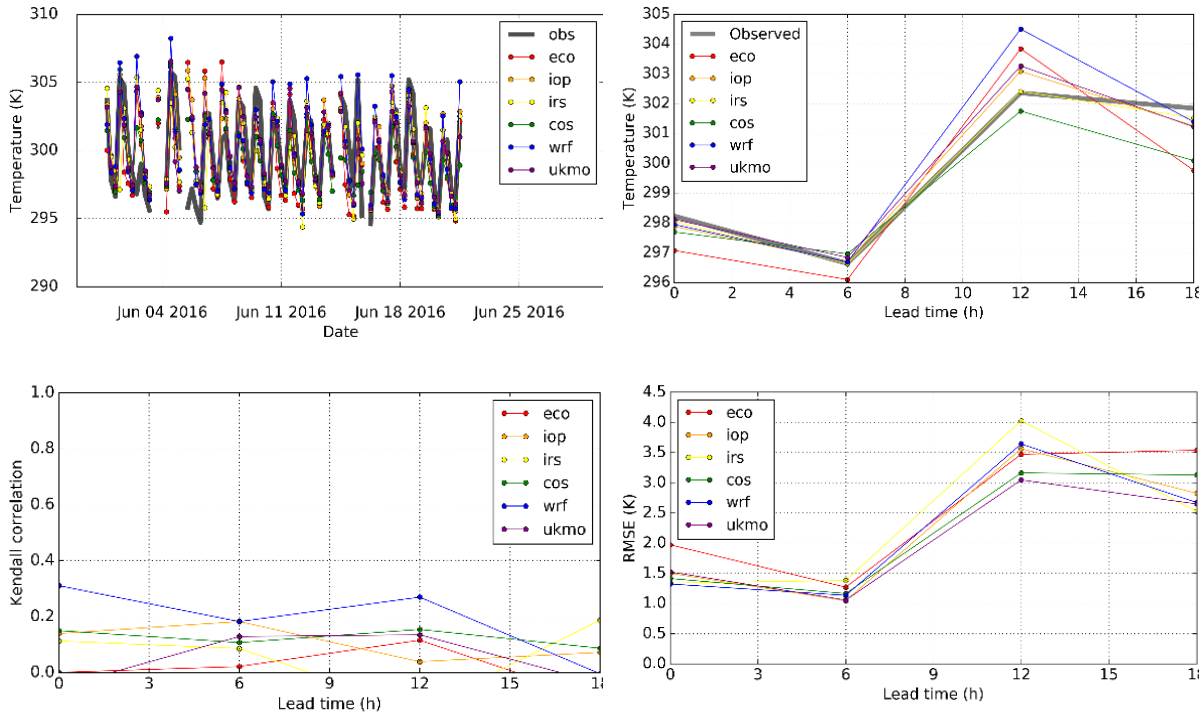

Figure 5: Example of standard verification analysis for temperature at 2m at the station of Parakou during the pre-onset period and for forecast Day 1. Top left: time series of absolute values; top right: mean diurnal cycle; bottom left: Kendall correlation coefficient for individual lead times (= times of day); bottom right: RMSE for individual lead times (=times of day). Different colours show different models according to the legend.

The statistics for a single station as discussed above can be summarized in RMSE plots and in Taylor diagrams (Figure 6). On the left hand side, the systematic and the unsystematic part of the RMSE are shown. The systematic error is the general shift of a modelled time-series to the observation, which can be created by fitting the model data with a linear regression to the observations and then subtracting the fit line from the one-to-one line. The unsystematic part is then the distance of the individual model data points from the fitted line. Therefore in this error plot the circles correspond to locations of equal total RMSE but the systematic and unsystematic part can vary. The closer the displayed points on a specific circle get to the x-axis, the better, since the systematic error is small in this case and a general shift cannot be observed. The results for Parakou reveal that the RMSE is dominated by the inability to reproduce local variations in temperature, while in comparison the found biases contribute significantly less.

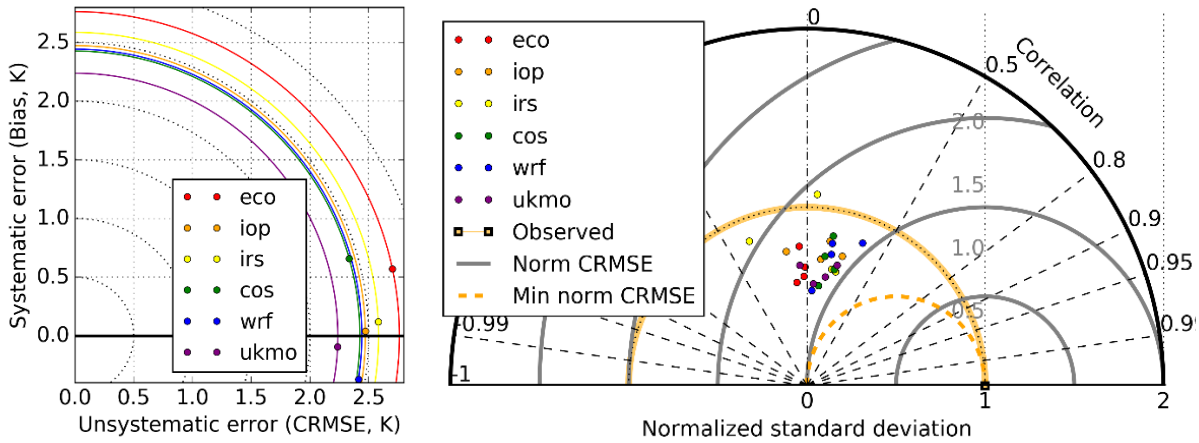

Figure 6: Example of summary verification diagrams for temperature at 2m at the station of Parakou during the pre-onset period and for forecast Day 1. Left: Error diagram with contributions from systematic and unsystematic errors to the RMSE with the different times of day combined. The latter is referred to as "centred root mean square error (CRMSE)". Right: Taylor diagram displaying correlations (as in bottom left panel of Figure 5) as the azimuthal angle (grey dashed lines) and forecast standard deviation normalized by the standard deviation of the observations on the x-axis (orange circle is standard deviation = 1, black circle standard deviation = 2). Individual points are different times of day. Lines of constant normalised CRMSE are given in grey.

The Taylor diagram on the right hand side of Figure 6 displays correlation between model forecasts and observations together with the normalized standard deviation in the model data. Grey lines show areas of constant normalised CRMSE. The performance of each model can be compared in terms of statistical measures in this way. In this example, all models show a low correlation (some are even anti-correlated) as discussed above, but most of them have a small CRMSE of about 1.2. The normalised standard deviation is for all models and all points in time (with the exception of one ICON research point) smaller than 1. This means that temporal variation of the temperature in the models is on average smaller than that of the measurements which reflects the difference between a point measurement (the station) and a box averaged variable (the models with certain grid sizes).

Comparing the plots explained and discussed above for the different stations reveals some interesting differences. Here we use the coastal stations Abidjan and Accra to illustrate possible problems of the models with coastal features. In Figure 7 the time-series of temperature for Abidjan (upper panel) and Accra (lower panel) are displayed together with the error measures. As can easily be seen, the model WRF has far lower temperatures than the observations and all other models in Abidjan. This is a typical problem when comparing station data with model grid boxes. The stations only represent one single point in space and close to the coast may not be representative for a larger region. The models, on the other hand, give values averaged over the size of the respective grid box. The location and form of the grid boxes are not the same for all models. ICON in the operational version for example was run with a triangular mesh with 13 km effective horizontal resolution, while WRF is based on a reduced Gaussian grid with 3 km horizontal resolution. As both grids do not have their boxes in the same locations, it is possible that the WRF grid box that includes Abidjan has more ocean in it than the ICON box. Since the ocean is colder than the surrounding land, this could lead to the observed deviations from the measurements. All other models in contrast show a much too low diurnal cycle in temperature, which could be related to an insufficiently represented land-sea breeze. These differences are clearly reflected in the systematic errors shown on the right hand side. In Accra the agreement is much better for all models, particularly for WRF, which shows one of the lowest total RMSE.

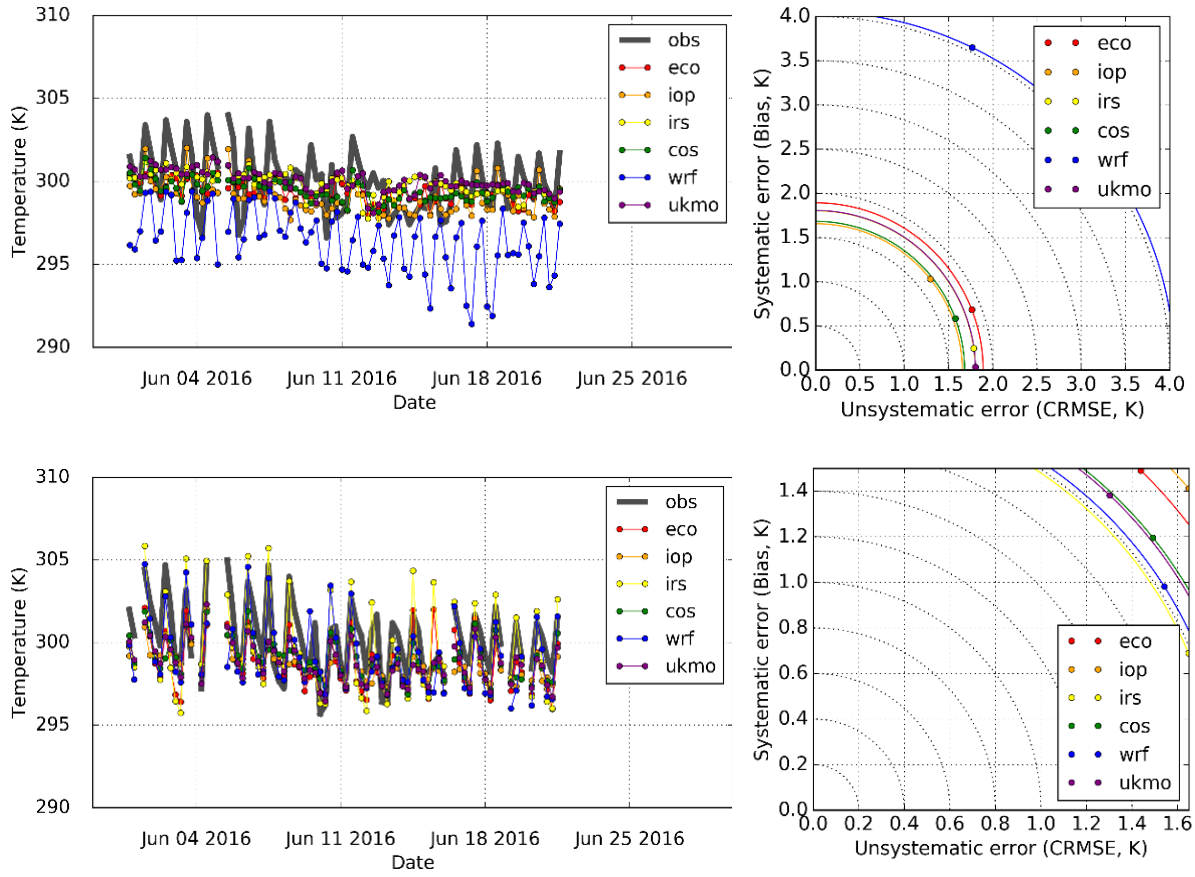

Figure 7: Illustration of problems with coastal features. Shown here are timeseries (left) and error diagrams (right) for temperature at 2m during the pre-onset period and for forecast Day 1. Top: Abidjan, bottom: Accra.

In addition, the various graphical analysis were compared for different meteorological variables. In Figure 8 the variables dew point temperature and wind speed at 10m above ground are shown with error plot and Taylor diagram again for the station at Parakou. For both variable, the total RMSE is the result of moderate biases of both signs combined with relatively large unsystematic errors, again likely related to local factors such as cloudiness and rain, which are not well represented by the models. This is also reflected by the very low (and sometimes even negative) correlations in the Taylor diagrams (right side in Figure 8). For most models, the dew point temperature is better represented than the 10m wind speed in a statistical sense because the correlations are higher and mainly positive. Additionally, the normalised CRMSE is smaller (closer to 1 instead of 1.5).

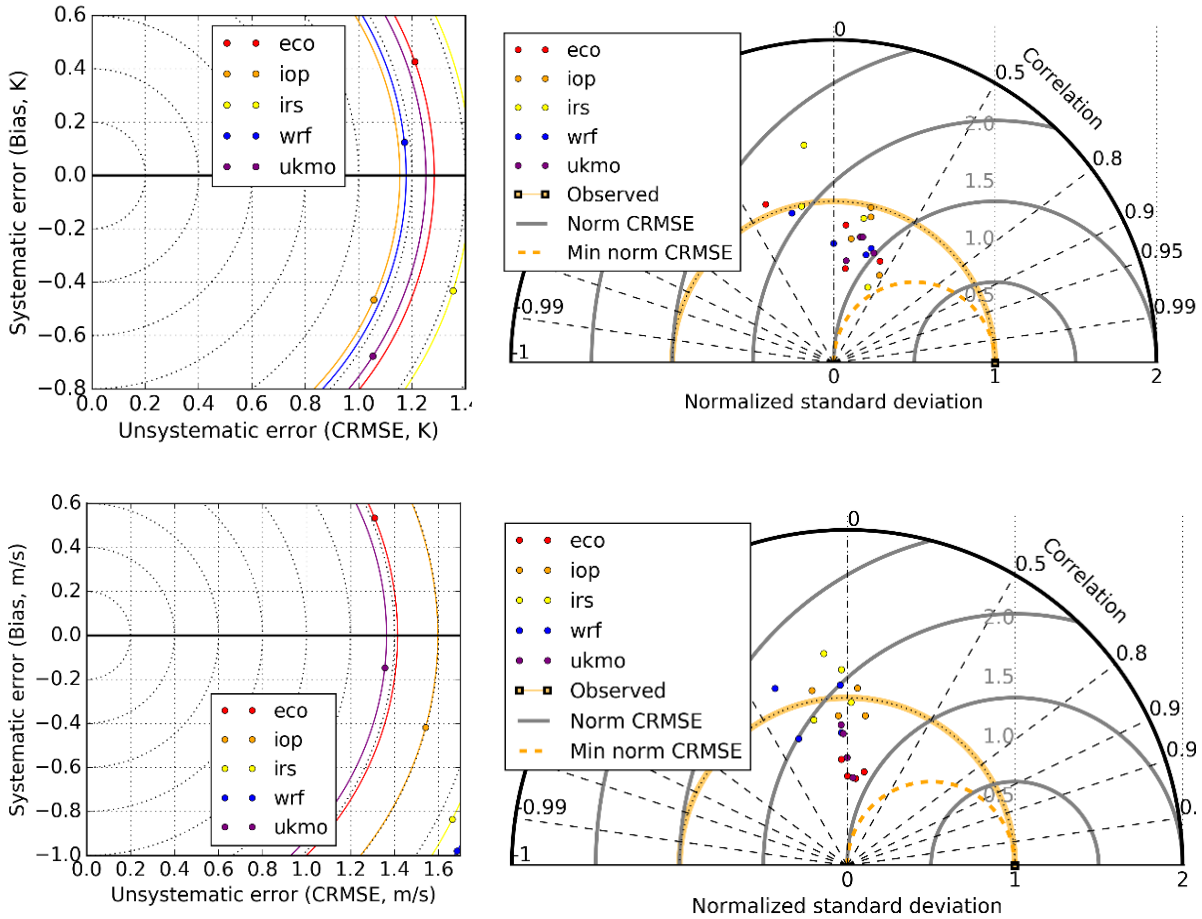

Figure 8: Summary verification diagrams at the station of Parakou during the pre-onset period and for forecast Day 1 as in Figure 6 but here for the variables dew point at 2m (top) and wind speed 10m (bottom).

In Figure 9 timeseries of precipitation and error diagrams for Parakou for the pre-onset and post-onset period are shown. It is clear that all models suffer from large uncertainties in the timing and amount of the precipitation both in the pre-onset and in the post-onset phases. The ECMWF model appears to have the lowest bias and the largest unsystematic error in both periods, with the exception of the COSMO model for period 2, while other models have more similar behaviours. It is worth noting that this type of analysis does not taken into account the spatial structure of the precipitating systems in the forecast. This may lead to large errors due for example to the wrong location of the system even for forecasts which are otherwise relatively skilful. This is especially problematic for high resolution models.

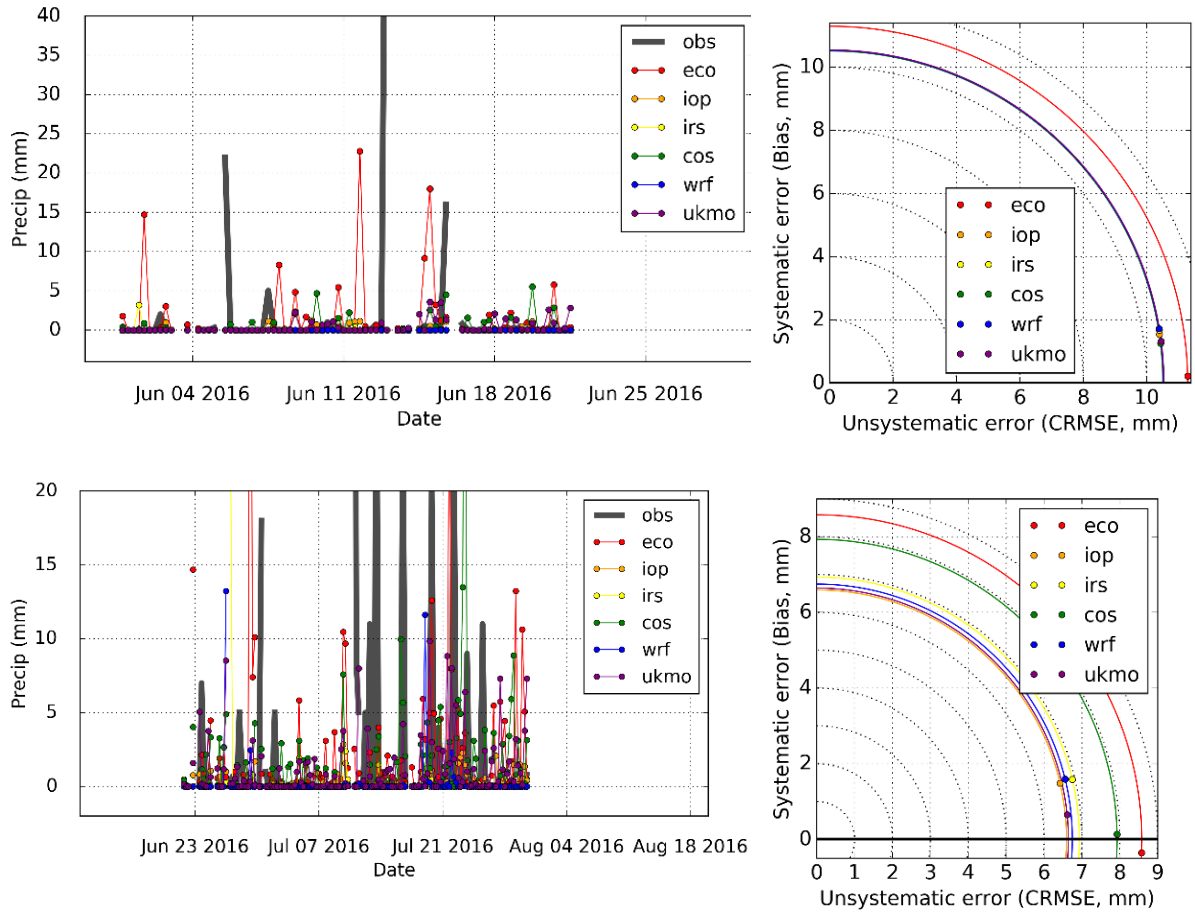

Figure 9: Illustration of problems with forecasting precipitation accurately in time, space and amount. Shown here are the Parakou timeseries (left) and error diagrams (right) for total precipitation during the pre-onset period (top) and the post-onset period (bottom) for forecast Day 1.

4.1.2 Radiosondes and wind profilers data

Radiosonde data collected during the DACCIWA campaign were made available via the Global Telecommunications Service (GTS) and picked up by operational centres, such as ECMWF for their meteorological analyses. Specifically at ECMWF some of the stations, for example Savé, were not processed due to a different reporting format (BUFR TEMP MOBILE), which is not yet recognized in the operations and were not archived. Other stations reported in standard BUFR. Those were stored in the ECMWF MARS archive and retrieved for the evaluation.

Here exemplarily, temperature and wind speed at two different stations (Cotonou and Abidjan) were plotted. These are shown in Figure 10 and Figure 11, respectively. Overall the models do a good job in reproducing the observed average profiles of temperature, even though the finer structures, which are present in the observed profiles are not captured. Particularly during the post-onset phase in Cotonou some relatively marked spikes are seen in the observations, that could also come from faulty measurements. At the surface a more substantial bias of few degrees is present. The reasons for this need more detailed study in the future.

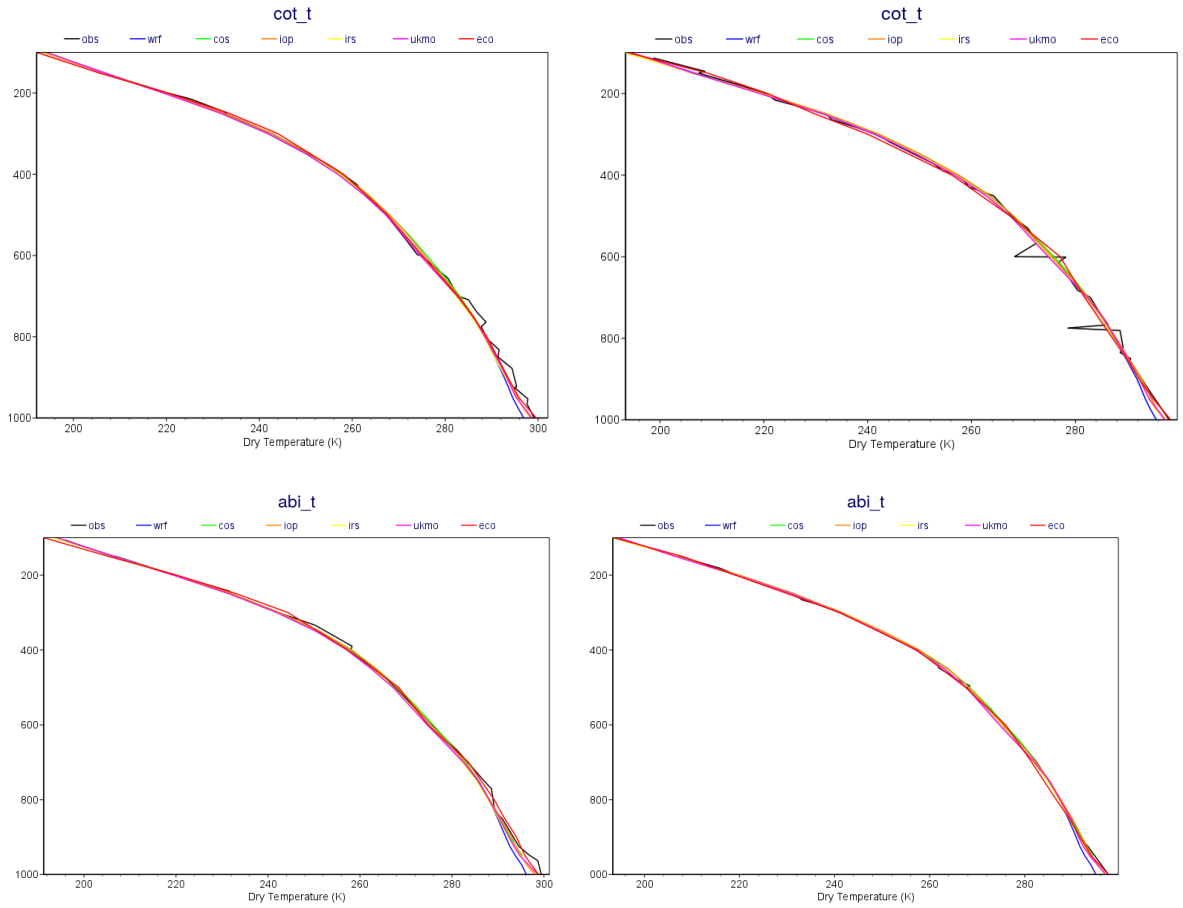

Figure 10: Average profiles of dry bulb temperature (K) for the pre-onset (left) and post onset (right) period compared with TEMP temperature observations at Cotonou (top) and Abidjan (bottom). Vertical axis shows pressure in hPa. Observations are in black. Plots courtesy of Fernando Ii (ECMWF).

For wind speed, however, the discrepancies between model and observations become more evident leading to large biases particularly for upper levels. Again the reasons for some of the more pronounced spikes in the observations need some closer inspection in cooperation with WP6 that coordinated the radiosonde campaign. It is possible that larger deviations could come from the outflow of individual convective systems, which we cannot expect the models to reproduce. One of the most interesting meteorological features for DACCIWA is the low-level jet around 925 hPa. As expected, this feature increases from the pre- to the post-onset period (compare left and right panels in Figure 11). While most of the models considered appear to reproduce the jet quite realistically, WRF shows a substantial overestimation similar to many climate models (see Hannak et al. 2017).

Another characteristic change from pre- to post-onset is the northward shift of the African easterly jet around 600 hPa. At Cotonou the pre-onset jet speed is underestimated by all models, while at Abidjan the observations show a suspicious absence of the jet, which again needs additional checks in collaboration with WP6. Agreement in mid-level winds after the onset is better at both stations and for all models.

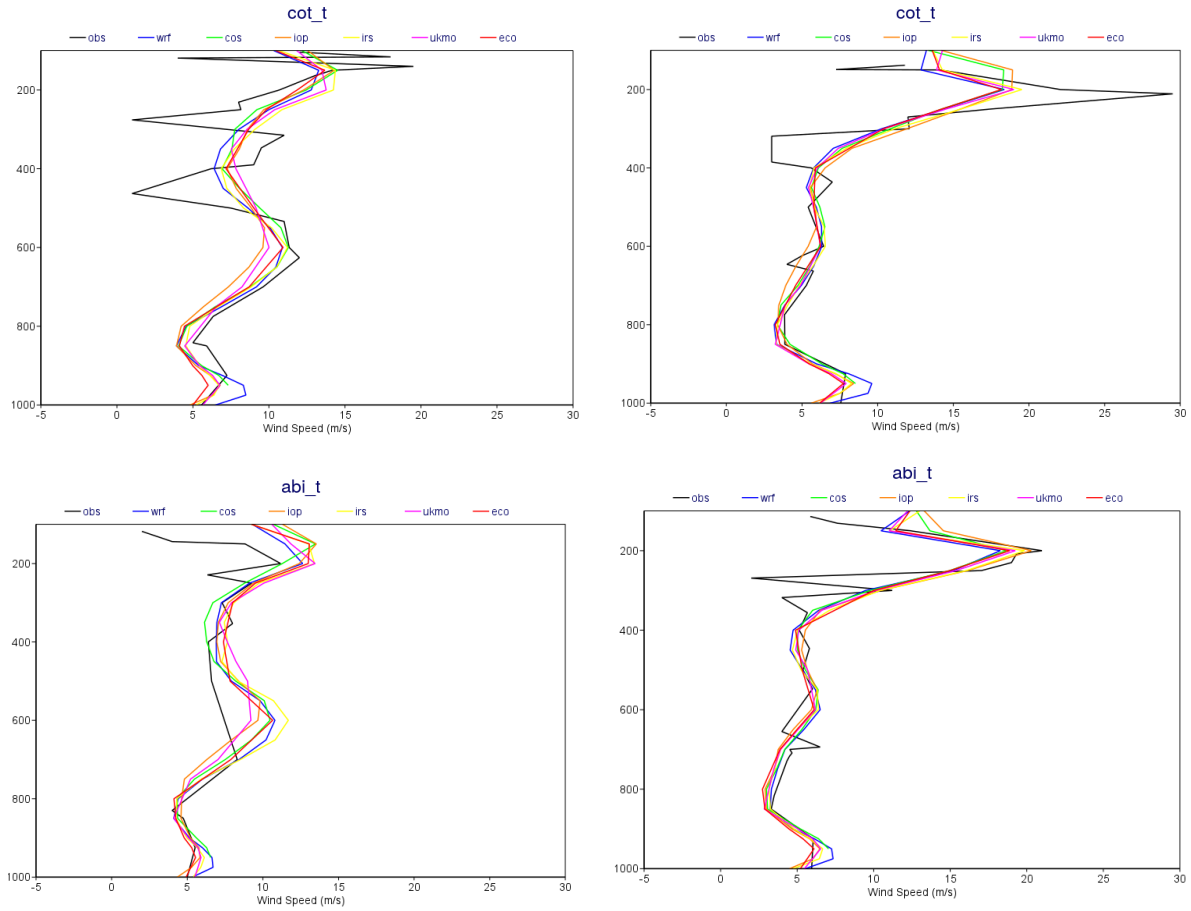

Figure 11: Average profiles of wind speed (m/s) for the pre-onset (left) and post onset (right) period compared with TEMP wind observations at Cotonou (top) and Abidjan (bottom).

4.1.3 Box averages

Additionally to the station data analysis, the model forecasts were analysed in terms of average performance over the box of interest (8°W–8°E, 5–10°N) highlighted in Figure 3.

For precipitation, satellite data from the Global Precipitation Climatology Centre (GPCC) were post-processed in a similar way to the models and with the same spatial resolution. The GPCC horizontal resolution is one degree, the 0.2 degree files used here are thus a result of interpolation. GPCC temporal resolution is daily, so there are no diurnal cycles and the files cover the period from 00.00 – 23.59 UTC. These two factors could partially explain differences between the models and observations. Figure 12 shows precipitation timeseries and errors for the pre-onset (top) and post-onset (bottom) periods. These comparisons show that generally all models do better in a spatial-average sense than at individual stations (cf. Figure 4 and Figure 9). The variability is reasonably represented. Overall biases are in an acceptable range except for WRF that underestimates rainfall significantly. Models struggle to represent day-to-day variations leading to a relatively large CRMSE, particularly in the pre-onset period.

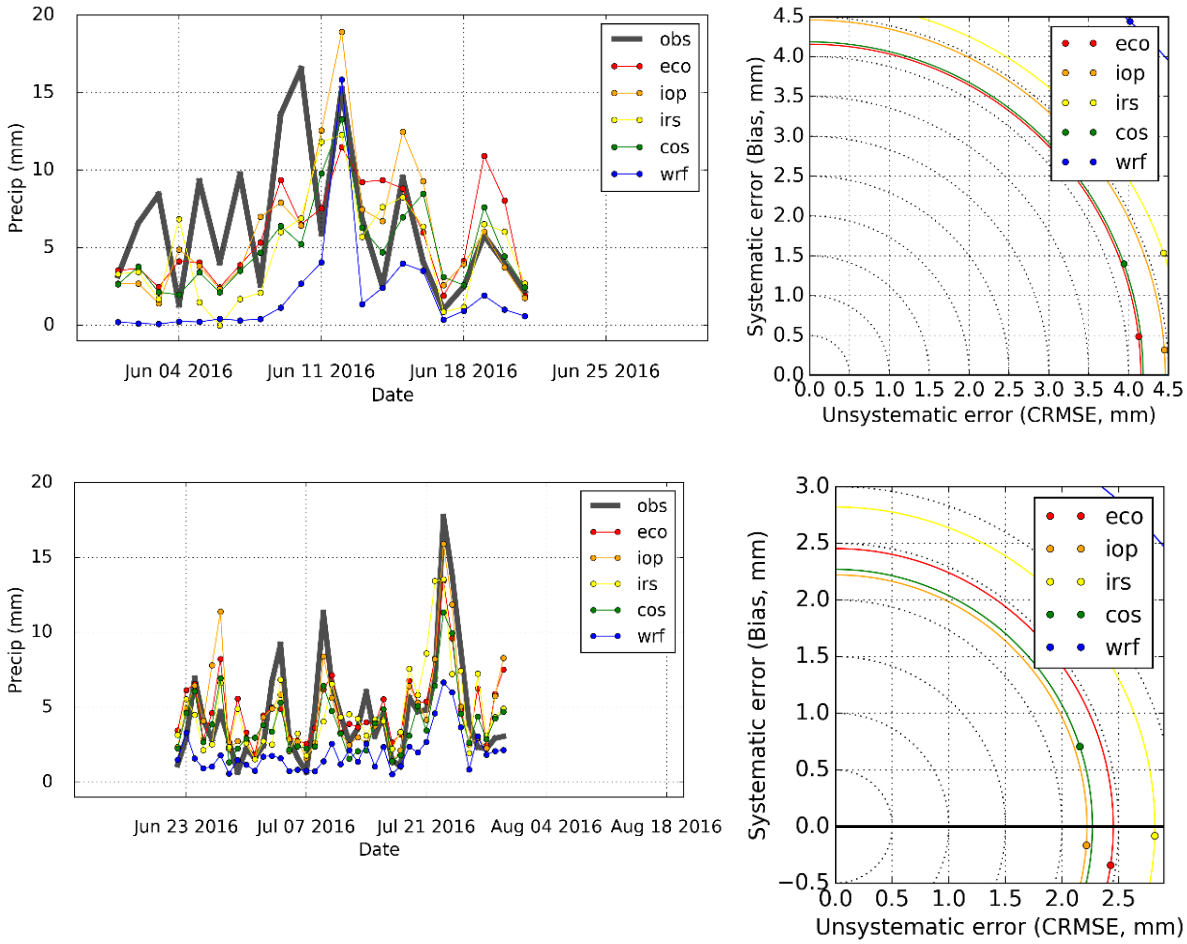

Figure 12: Box-average precipitation from the various models compared with GPCC observations. Time-series are shown on the left and errors on the right. Top: pre-onset period; Bottom: post-onset period.

An additional variable which was verified using independent satellite data was Outgoing Longwave Radiation (OLR), often connected with convective precipitation. For this evaluation measurements from Geostationary Earth Radiation Budget (GERB) instrument processed at the University of Reading were used.

GERB measurements were averaged of the preceding three hours, calculated from measurements every 15 minutes. To avoid biasing the fluxes due to diurnal sampling, if any GERB data in the three hour window was missing, the three hour average was set to missing. GERB solar flux suffers from sun-glint over water surfaces at low zenith angles, which means that these are often missing. Note that when sun glint occurs, the daily means are biased low because it occurs at low zenith angles. GERB solar flux is only measured for zenith angles less than 80 degrees. The data were extended to 104.5 degrees using CERES twilight measurements and interpolation as described in Hill et al (2016).

Figure 13 shows OLR timeseries and errors for the pre-onset and post-onset periods. Most models have a lower bias in the post-onset period than in the pre-onset but large CRMSE in both period. A small exception is the COSMO model which display a large bias in the post-onset period, possibly connected with an underestimation of cirrus outflow resulting from deep convection (to be confirmed).

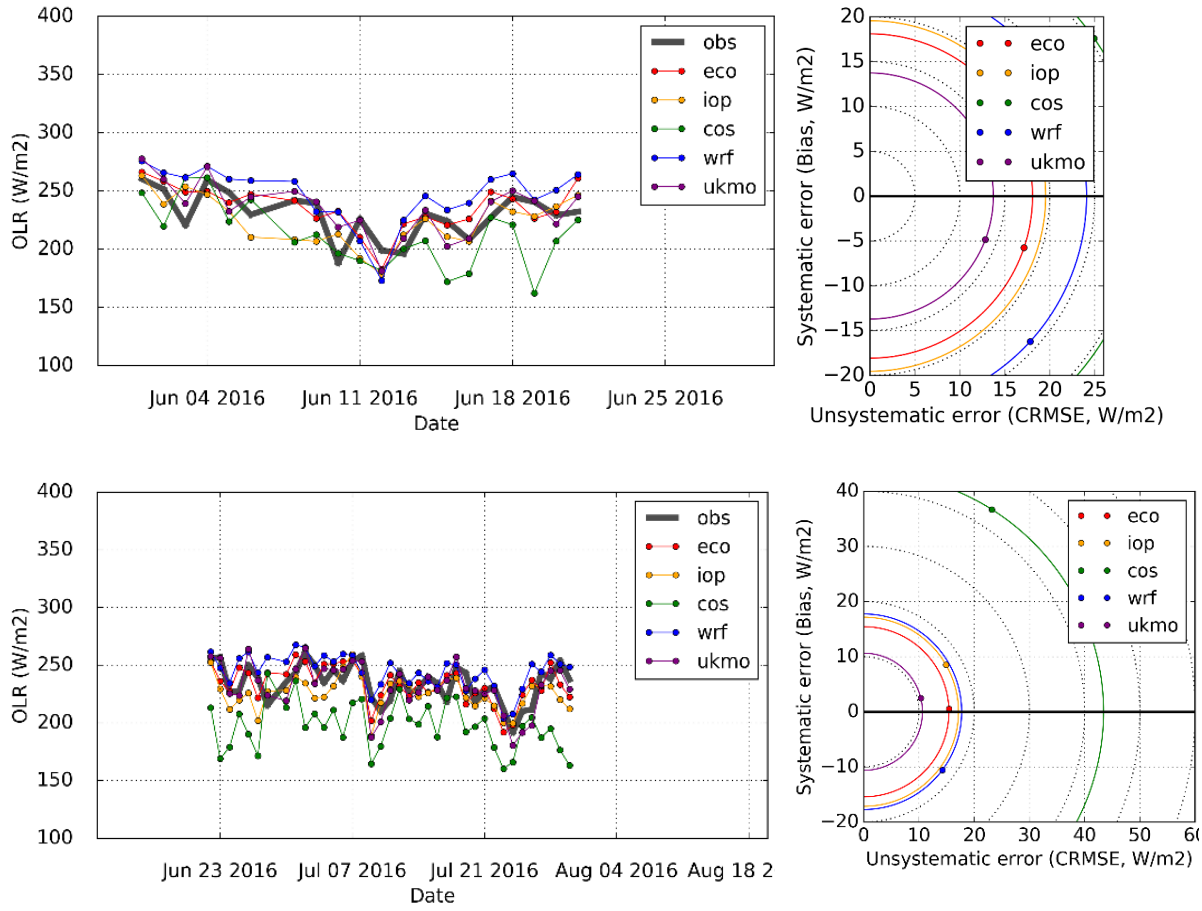

Figure 13: Box-average OLR from the various models compared with GERB observations. Time-series are shown on the left and errors on the right. Top: pre-onset period; Bottom: post-onset period.

5 Conclusions

This report summarises the concept and some first results from the comprehensive forecast evaluation exercise conducted as part of the DACCIWA field campaign in June-July 2016. To the best of our knowledge, this is the first study of this kind that comprises a wide range of state-of-the-art models run in operational and research configurations and representing convection explicitly or through parameterisation. Before the actual computations a detailed strategy was developed and protocols for data processing and sharing were established. Through this process all model and observational data were handled in a consistent and thus fully comparable way. For the computation of standard metrics and graphical displays, an operational software package used at ECMWF was employed.

The first results have revealed some satisfactory skill in some models for some meteorological variables (e.g. representation of low-level jet) but also a number of substantial problems, particularly to do with coastal features, precipitation and day-to-day variations in cloudiness, boundary-layer evaluation and temperature. The next months will be used to evaluate this rich resource more systematically to draw final conclusions about the models' capabilities and deficits. The analysis has also revealed some observational issues that need to be resolved with the data producers within DACCIWA. It is planned to turn this work into a journal publication once the analysis is fully completed at a scientific level.

6 References

General

Hannak, L., P. Knippertz, A.H. Fink, A. Kniffka, and G. Pante, 2017: Why Do Global Climate Models Struggle to Represent Low-Level Clouds in the West African Summer Monsoon?. J. Climate, 30, 1665–1687, doi: 10.1175/JCLI-D-16-0451.1.

Hill, P. G., R. P. Allan, J. C. Chiu, and T. H. M. Stein (2016), A multisatellite climatology of clouds, radiation, and precipitation in southern West Africa and comparison to climate models, J. Geophys. Res. Atmos., 121, 10,857–10,879, doi:10.1002/ 2016JD025246.

Knippertz, P.; Fink, A. H.; Deroubaix, A.; Morris, E.; Tocquer, F.; Evans, M.; Flamant, C.; Gaetani, M.; Lavaysse, C.; Mari, C.; Marsham, J. H.; Meynadier, R.; Affo-Dogo, A.; Bahaga, T.; Brosse, F.; Deetz, K.; Guebsi, R.; Latifou, I.; Maranan, M.; Rosenberg, P. D.; Schlueter, A., 2017: A meteorological and chemical overview of the DACCIWA field campaign in West Africa in June–July 2016. Atmos. Chem. Phys. Disc., doi:10.5194/acp-2017-345

Novella, N. S., and W. M. Thiaw (2013), African rainfall climatology version 2 for early warning systems, J. Appl. Meteorol. Climatol., 52, 588–606.

References (COSMO-ART)

Athanasopoulou, E., Vogel, H., Vogel, B., Tsimpidi, A., Pandis, S. N., Knote, C., and Fountoukis, C., 2013: Modeling the meteorological and chemical effects of secondary organic aerosol during an EUCAARI campaign, Atmos. Chem. Phys., 13, 625-645, doi:10.5194/acp-13-625-2013.

Athanasopoulou, E., Rieger, D., Walter, C., Vogel, H., Karali, A., Hatzaki, M., Gerasopoulos, E., Vogel, B., Giannakopoulos, C., Gratsea, M., and Roussos, A., 2014: Fire risk, atmospheric chemistry and radiative forcing assessment of wildfires in eastern Mediterranean, Atmos. Environ., 95, 113–125, doi:10.1016/j.atmosenv.2014.05.077.

Baldauf, M., Seifert, A., Förstner, J., Majewski, D., Raschendorfer, M., and Reinhardt, T., 2011: Operational convective-scale numerical weather prediction with the COSMO model: description and sensitivities, Mon. Weather Rev., 139, 3887–3905, doi:10.1175/MWR-D-10-05013.1.

Barahona, D. and Nenes, A., 2009a: Parameterizing the competition between homogeneous and heterogeneous freezing in cirrus cloud formation – monodisperse ice nuclei, Atmos. Chem. Phys., 9, 369–381, doi:10.5194/acp-9-369-2009.

Barahona, D. and Nenes, A., 2009b: Parameterizing the competition between homogeneous and heterogeneous freezing in ice cloud formation – polydisperse ice nuclei, Atmos. Chem. Phys., 9, 5933–5948, doi:10.5194/acp-9-5933-2009.

EDGAR, 2010: http://edgar.jrc.ec.europa.eu/htap_v2/index.php?SECURE=123

Fountoukis, C. and Nenes, A., 2005: Continued development of a cloud droplet formation parameterization for global climate models, J. Geophys. Res.-Atmos., 110, D11212, doi:10.1029/2004JD005591.

GFAS, 2016: http://apps.ecmwf.int/datasets/data/cams-gfas/

Guenther, A. B., Jiang, X., Heald, C. L., Sakulyanontvittaya, T., Duhl, T., Emmons, L. K., Wang, X., 2012: The Model of Emission of Gases and Aerosols from nature version 2.1 (MEGAN2.1): an extended and updated framework of modelling biogenic emissions, Geosci. Model Dev., 5, 1471-1492.

Lana, A., Bell, T. G., Simó, R., Vallina, S. M., Ballabrera-Poy, J., Kettle, A. J., Dachs, J., Bopp, L., Saltzman, E. S., Stefels., J., Johnson, J. E., Liss, P. S., 2011: An updated climatology of surface dimethylsulfide concentrations and emission fluxes in the global ocean, Global Biogeochemical Cycles, Vol. 25, GB1004.

Phillips, V. T., DeMott, P. J., and Andronache, C., 2008: An empirical parameterization of heterogeneous ice nucleation for multiple chemical species of aerosol, J. Atmos. Sci., 65, 2757–2783, doi:10.1175/2007JAS2546.1.

Riemer, N., H. Vogel, B. Vogel (2004), Soot aging time scales in polluted regions during day and night, Atmos. Chem. Phys., 4, 1885–1893, SRef-ID: 1680-7324/acp/2004-4-1885.

Ritter, B. and Geleyn, J.-F., 1992: A comprehensive radiation scheme for numerical weather prediction models with potential applications in climate simulations, Mon. Weather Rev., 120, 303–325, doi:10.1175/1520-0493(1992)120<0303:ACRSFN>2.0.CO;2.

Schuster, R., Fink, A. H., Knippertz, P., 2013: Formation and Maintenance of Nocturnal Low-Level Stratus over the Southern West African Monsoon Region during AMMA 2006, Journal of the Atmospheric Sciences, Vol. 70, 2337-2355.

Seifert, A. and Beheng, K., 2006: A two-moment cloud microphysics parameterization for mixed-phase clouds. part 1: Model description, Meteorol. Atmos. Phys., 92, 45–66, doi:10.1007/s00703-005-0112-4.

Shao, Y., Fink, A. H., Klose, M., 2010: Numerical simulation of a continental-scale Saharan dust event, Journal of Geophysical Research, Vol. 115, D13205.

Stanelle, T., Vogel, B., Vogel, H., Bäumer, D., and Kottmeier, C., 2010: Feedback between dust particles and atmospheric processes over West Africa during dust episodes in March 2006 and June 2007, Atmos. Chem. Phys., 10, 10771–10788, doi:10.5194/acp-10-10771-2010.

Stockwell, W. R., Middleton, P., Chang, J. S., and Tang, X., 1990: The second generation regional acid deposition model chemical mechanism for regional air quality modeling, J. Geophys. Res.-Atmos., 95, 16343–16367, doi:10.1029/JD095iD10p16343.

Rieger, D., Bangert, M., Kottmeier, C., Vogel, H., and Vogel, B., 2014: Impact of aerosol on post-frontal convective clouds over Germany, Tellus B, 66, 22528, doi:10.3402/tellusb.v66.22528.

Vogel, B., Vogel, H., Bäumer, D., Bangert, M., Lundgren, K., Rinke, R., Stanelle, T., 2009: The comprehensive model system COSMO-ART - Radiative impact of aerosol on the state of the atmosphere on the regional scale, Atmos. Chem. Phys., 9, 8661-8680.

Walter, C., Freitas, S. R., Kottmeier, C., Kraut, I., Rieger, D., Vogel, H., Vogel, B. (2016): The importance of plume rise on the concentrations and atmospheric impacts of biomass burning aerosol, Atmos. Chem. Phys., 16, 9201-9219.

References (ICON)

Barker H. W., A. Marshak, W. Szymer, A. P. Trishchenko, J.-P. Blanchet, Z. Li, 2002: Inference of cloud optical depth from aircraft-based solar radiometric measurements. Journal of Atmospheric Sciences. 59, 2093-2111.

Bechtold P, Köhler M, Jung T, Doblas-Reyes F, Leutbecher M, Rodwell M, Vitart F, Balsamo G. 2008. Advances in simulating atmospheric variabilitywith the ECMWF model: From synoptic to decadal time-scales. Q. J. R. Meteorol. Soc. 134: 1337–1351.

Doms, G. and U. Schättler, 2004: A description of the nonhydrostatic regional model LM. Part II: Physical parameterization. Technical report, Deutscher Wetterdienst, Offenbach, (available from http://www.cosmomodel.org/public/documentation.htm).

Heise E, Ritter B, Schrodin E. 2006. 'Operational implementation of the multilayer soil model TERRA', Technical report. Deutscher Wetterdienst: Offenbach, Germany. http://www.cosmo-model.org.

Leuenberger D, Koller M, Fuhrer O, Schär C. 2010. A generalization of theSLEVE vertical coordinate. Mon. Weather Rev. 138: 3683–3689.

Lott F, Miller M. 1997. A new subgrid-scale orographic drag parametrization: Its formulation and testing. Q. J. R. Meteorol. Soc. 123: 101–127.

Mlawer EJ, Taubman SJ, Brown PD, Iacono MJ, Clough SA. 1997. Radiative transfer for inhomogeneous atmospheres: RRTM, a validated correlated-k model for the longwave. J. Geophys. Res. 102: 16 663–16 682, doi:10.1029/97JD00237.

Orr A, Bechtold P, Scinocca J, Ern M, Janiskova M. 2010. Improved middle atmosphere climate and forecasts in the ECMWF model through a nonorographic gravity wave drag parameterization. J. Clim. 23: 5905–5926.

Raschendorfer M. 2001. The new turbulence parameterization of LM. COSMO Newsl. 1: 89–97. http://www.cosmo-model.org.

Seifert A. 2008. A revised cloud microphysical parameterization for COSMO–LME. COSMO Newsl. 8: 25–28. http://www.cosmo-model.org.

Zängl, G., Reinert, D., Rípodas, P. and Baldauf, M., 2015: The ICON (ICOsahedral Non-hydrostatic) modelling framework of DWD and MPI-M: Description of the non-hydrostatic dynamical core. Q.J.R. Meteorol. Soc., 141, 563–579, doi:10.1002/qj.2378.

References (MetUM)

Bellouin, N., Rae, J., Jones, A., Johnson, C., Haywood, J., and Boucher, O. (2011): Aerosol forcing in the Climate Model Intercomparison Project (CMIP5) simulations by HadGEM2-ES and the role of ammonium nitrate, J. Geophys. Res., 116, D20206, doi:10.1029/2011JD016074.

Best, M., Pryor, M., Clark, D., Rooney, G., Essery, R., Ménard, C., Edwards, J., Hendry, M., Porson, A., Gedney, N., Mercado, L., Sitch, S., Blyth, E., Boucher, O., Cox, P., Grimmond, C., and Harding, R. (2011): The Joint UK Land Environment Simulator (JULES), model description – Part 1: Energy and water fluxes, Geosci. Model Dev., 4, 677–699, doi:10.5194/gmd-4-677-2011.

Brown, A., Milton, S., Cullen, M., Golding, B., Mitchell, J., and Shelly, A. (2012): Unified Modeling and Prediction of Weather and Climate: A 25-Year Journey, Bull. Amer. Meteor. Soc., 93, 1865–1877, doi:10.1175/BAMS-D-12-00018.1.

Clayton, A., Lorenc, A., and Barker, D. M. (2012): Operational implementation of a hybrid ensemble/4D-Var global data assimilation system at the Met Office, Quart. J. Roy. Meteor. Soc., doi:10.1002/qj.2054.

Cullen, M. and Davies, T. (1991): A conservative split-explicit integration scheme with fourth-order horizontal advection, Quart. J. Roy. Meteor. Soc., 117, 993–1002, doi:10.1002/qj.49711750106.

Dharssi, I., Bovis, K., Macpherson, B., and Jones, C. (2011): Operational assimilation of ASCAT surface soil wetness at the Met Office,Hydro. Earth Sys. Sci., 15, 2729–2746, doi:10.5194/hess-15-2729-2011.

Gregory, D. and Rowntree, P. R. (1990): A massflux convection scheme with representation of cloud ensemble characteristics and stability dependent closure, Mon. Weather Rev., 118, 1483–1506, doi:10.1175/1520-0493(1990)118<1483:AMFCSW>2.0.CO;2.

Rawlins, F., Ballard, S. P., Bovis, K. J., Clayton, A. M., Li, D., Inverarity, G. W., Lorenc, A. C., and Payne, T. J. (2007): The Met Office global four-dimensional variational data assimilation scheme, Quart. J. Roy. Meteor. Soc., 133, 347–362, doi:10.1002/qj.32.

Walters, D., Brooks, M., Boutle, I., Melvin, T., Stratton, R., Vosper, S., Wells, H., Williams, K., Wood, N., Allen, T., Bushell, A., Copsey, D., Earnshaw, P., Edwards, J., Gross, M., Hardiman, S., Harris, C., Heming, J., Klingaman, N., Levine, R., Manners, J., Martin, G., Milton, S., Mittermaier, M., Morcrette, C., Riddick, T., Roberts, M., Sanchez, C., Selwood, P., Stirling, A., Smith, C., Suri, D., Tennant, W.,

Vidale, P.L., Wilkinson, J., Willett, M., Woolnough, S. & Xavier, P. (2016).: The Met Office Unified Model Global Atmosphere 6.0/6.1 and JULES Global Land 6.0/6.1 configurations, Geosci. Model Dev, doi:10.5194/gmd-2016-194.

Wood, N., Staniforth, A., White, A., Allen, T., Diamantakis, M., Gross, M., Melvin, T., Smith, C., Vosper, S., Zerroukat, M., and Thuburn, J. (2014): An inherently mass-conserving semi-implicit semi-Lagrangian discretization of the deep-atmosphere global non-hydrostatic equations, Q. J. Roy. Meteorol. Soc., 140, 1505–1520, doi:10.1002/qj.2235.

Woodward, S, (2001): Modeling the atmospheric life cycle and radiative impact of mineral dust in the Hadley Centre climate model, J. Geophys. Res. 106, doi:10.1029/2000JD900795.

References (WRF)

Chen, F., & Dudhia, J. (2001). Coupling an advanced land surface–hydrology model with the Penn State–NCAR MM5 modeling system. Part I: Model implementation and sensitivity. Monthly Weather Review, 129(4), 569-585.

Mlawer EJ, Taubman SJ, Brown PD, Iacono MJ, Clough SA. 1997. Radiative transfer for inhomogeneous atmospheres: RRTM, a validated correlated-k model for the longwave. J. Geophys. Res. 102: 16 663–16 682, doi:10.1029/97JD00237.

Morrison, H., & Gettelman, A. (2008). A new two-moment bulk stratiform cloud microphysics scheme in the Community Atmosphere Model, version 3 (CAM3). Part I: Description and numerical tests. Journal of Climate, 21(15), 3642-3659.

Nakanishi, M., & Niino, H. (2009). Development of an improved turbulence closure model for the atmospheric boundary layer. Journal of the Meteorological Society of Japan. Ser. II, 87(5), 895-912.

Schröder, M., König, M., & Schmetz, J. (2009). Deep convection observed by the Spinning Enhanced Visible and Infrared Imager on board Meteosat 8: Spatial distribution and temporal evolution over Africa in summer and winter 2006. Journal of Geophysical Research: Atmospheres, 114(D5).

Schuster, R., Fink, A. H., & Knippertz, P. (2013). Formation and maintenance of nocturnal low-level stratus over the southern West African monsoon region during AMMA 2006. Journal of the Atmospheric Sciences, 70(8), 2337-2355.

Skamarock, W. C., Klemp, JB., Duddhia, J., Barker DM., Duda, MG., Huang XY., Wang W., Powers JG., (2008): A Description of the Advanced Research WRF Version 3. NCAR Technical Note NCAR/TN-475+STR, doi:10.5065/D68S4MVH.

7 Appendix 1: Evaluation protocol

Area: 8°W–8°E, 5–10°N

Grid: 0.2° x 0.2°

Pressure levels: 100, 150, 200, 250, 300, 350, 400, 450, 500, 550, 600, 650, 700, 750, 800, 850, 900, 925, 950, 975, 1000

CODE for file names: typ_par_perX_dat_tim_spa.n

typ

obs, fc1, fc2 (3)

The idea is to only use model runs started at 12 UTC and allow a spin-up of 6h. Thus, fc1 is D0_18UTC–D1_18UTC (or + 6h to +30h) and fc2 is D1_18UTC–D2_18UTC (+30h to +54h). This also implies that diurnal averages will always run from 18UTC–18UTC the following day. We propose to label that period with the latter day, not the former, e.g. 5 June runs from 18 UTC on the 4th to 18 UTC on the 5th.

par

2D: pre, lwp, iwp, (ctt), tpw, ssr, tt2, td2, v10, slp, olr, osr (12)

- pre: total precipitation (mm/h, averaged over preceding 3h)
- lwp: liquid water path (g/m2, instantaneous)
- iwp: ice water path (g/m2, instantaneous)
- ctt: cloud top temperature (K, instantaneous)
- tpw: total precipitable water (mm, instantaneous)
- ssr: downwelling surface SW irradiance (W/m2, averaged over preceding 3h)
- tt2: 2m temperate (K, instantaneous)
- td2: 2m dewpoint temperate (K, instantaneous)
- v10: 10m wind speed (m/s, instantaneous)
- slp: mean sea-level pressure (hPa, instantaneous)
- olr: outgoing LW radiation (W/m2, averaged over preceding 3h)
- osr: outgoing SW radiation (W/m2, averaged over preceding 3h)

3D: cfr, lwc, iwc, ttt, qqq, rhu, vuu, vvv, vab, zzz (10)

- cfr: cloud fraction ([0–1], instantaneous)
- lwc: liquid water content (g/m3, instantaneous)
- iwc: ice water content (g/m3, instantaneous)
- ttt: temperature (K, instantaneous)
- qqq: specific water vapour (g/kg, instantaneous)
- rhu: relative humidity (%, instantaneous)

- vuu: zonal wind component (m/s, instantaneous)

- vvv: meridional wind component (m/s, instantaneous)

- vws: wind speed (m/s, instantaneous)

All data on agreed list of standard pressure levels (in hPa): 1000, 950, ….?

3Dtend: (only for models wrf, irs, ecr, um4, see list below) (?)

- list of tendency terms

In Hannak et al.2017 we combined the different terms from the various models to finally obtain temperature tendencies from diffusion (PBL, gravity wave, subscale orography, depending on the model), convection (shallow, deep, gridscale), radiation (SW & LW) plus advection (from dynamical core). For moisture and momentum, the same but without the radiation part.

per

per1, per2 (2)

The original idea was to simply use June and July as the two periods. Based on the ACP met overview paper we are working on, it may make more sense to distinguish pre-monsoon (per1, 1–21 June) and post-monsoon (22 June – 31 July). The first period would begin with the forecast started at 12 UTC on 30 May but only Day 2 would be used. The second forecast would be the one started at 12 UTC on 31 May and both forecast days would be used. The last datasets would be forecasts started at 12 UTC on 19 June (both days) and on 20 June (only Day 1). In total this gives forecasts for the 21 days with 1 or 2 day lead times. Strictly speaking the periods would run from 18 UTC 31 May – 18 UTC 21 June. Similar rules would apply for the second period.

dat

mod: wrf, cos, irs, iop, eco, ecr, era, um4, uma, umko (10)

- wrf: Marlon’s WP6 runs

- cos: Konrad’s COSMO-ART runs

- irs: ICON research

- iop: ICON operational

- eco: ECMWF IFS operational

- um4: UM 4km run by Phil

- uma: UM with aerosol run by Malcolm

- umko: UM operational

obs

tim

3hh, dca/dcs, dav, pra/prs (4+2)

- 3hh: 3-hourly data (instantaneous or averaged, see variable list above)

- dca/dcs: averaged diurnal cycle + its standard deviation computed over PerX

- dav: daily average (18 UTC – 18 UTC, see above)

- pra/prs: average for whole period + its standard deviation computed from daily averages (dav)

spa

2D: hor, bxa, sit (supersites, SYNOP will be extracted directly by ECMWF)

- hor: horizontal field on standard 0.2°x0.2° grid

- bxa: spatial average over box 8°W–8°E, 5–10°N

3D: bpr, lpf, sav, kum, ile, abi, lam, acc, cot, par (10)

- bpr: box-averaged vertical profile on standard pressure levels

- lpf: latitude-pressure field averaged 8°W–8°E

- sav: grid box containing Savé (2.4281°E, 8.0001°N)

- kum: grid box containing Kumasi (1.5605’°W, 6.6802°N)

- ile: grid box containing Ile-Ife (4.5574°E, 7.5532°N)

- abi: grid box containing Abidjan (3.9229°W, 5.2736°N)

- lam: grid box containing Lamto (5.0265°W, 6.2235°N)

- acc: grid box containing Accra (0.1649°W, 5.6515°N)

- cot: grid box containing Cotenou (2.3885°E, 6.3566°N)

- par: grid box containing Parakou (2.6130°E, 9.3578°N)

What should be sent to ECMWF

2D fields

3h, 61 days, 48h forecasts, all parameters, standard 0.2° grid, SWA box

So an example file name could be **fc1_tt2_per2_um4_3hh_hor.nc** (2m temperature, 3 hourly data for forecast day 1 during the second period from the UM 4km run on a 0.2° horizontal grid)

3D fields

3h, 61 days, 48h forecasts, all parameters, box average, latitude-pressure fields and supersite and radiosonde stations as listed above

So an example file name could be **fc2_ttt_per1_wrf_3hh_lpf.nc** (temperature, 3 hourly data for forecast day 2 during the first period from WRF on a 0.2° latitude grid on standard pressure levels)

Types of plots / scores

As far as possible, plot names should follow the naming convention established above.

A) 2-D fields

1) Table with box averages of 2D fields

(10mod*2fc + 2obs)*12par*2per = 528 (average + std)

2) Time series daily 2D fields (met. param vs. 61 days in JJ16, all models & obs in one plot)

- box average: 2fc*12par = 24

- supersites: 2fc*12par*3sites = 72

3) Mean diurnal cycle of 2D fields (met. param vs. 8 times of day)

- box average: 2fc*12par*2per = 48

- SYNOPS: 2fc*5par*2per = 20 (averaged over all stations, MAE)

4) 2D horizontal distributions selected after analysis of plots 1)–3)

B) 3-D fields

1) Mean diurnal cycle profiles (met. param. vs. height)

- box average: 2fc*8timesofday*2per*5par = 160

- box averaged tendencies: 2fc*8timesofday*2per*4mod = 128

- RS sites: 2fc*4timesofday*1per(only 2.)*3par*9stations < 216

2) Latitude-pressure section

- 8W–8E average: 2fc*2per*5par*10mod = 200 (any obs?? GEOPROF)

Processing flow